



City Research Online

City, University of London Institutional Repository

Citation: Kappos, A.J., Gkatzogias, K.I. & Gidaris, I.G. (2013). Extension of direct displacement-based design methodology for bridges to account for higher mode effects. *Earthquake Engineering and Structural Dynamics*, 42(4), pp. 581-602. doi: 10.1002/eqe.2229

This is the submitted version of the paper.

This version of the publication may differ from the final published version.

Permanent repository link: <https://openaccess.city.ac.uk/id/eprint/3559/>

Link to published version: <https://doi.org/10.1002/eqe.2229>

Copyright: City Research Online aims to make research outputs of City, University of London available to a wider audience. Copyright and Moral Rights remain with the author(s) and/or copyright holders. URLs from City Research Online may be freely distributed and linked to.

Reuse: Copies of full items can be used for personal research or study, educational, or not-for-profit purposes without prior permission or charge. Provided that the authors, title and full bibliographic details are credited, a hyperlink and/or URL is given for the original metadata page and the content is not changed in any way.

City Research Online:

<http://openaccess.city.ac.uk/>

publications@city.ac.uk

Extension of direct displacement-based design methodology for bridges to account for higher mode effects

Andreas J. Kappos¹, Konstantinos I. Gkatzogias¹ and Ioannis G. Gidaris¹

¹Aristotle University of Thessaloniki, Civil Engineering Department, Laboratory of Reinforced Concrete & Masonry Structures, 54124 Thessaloniki, Greece

SUMMARY

An improvement is suggested to the direct displacement-based design (DDBD) procedure for bridges to account for higher mode effects, the key idea being not only the proper prediction of a target-displacement profile through the effective mode shape (EMS) method (wherein all significant modes are considered), but also the proper definition of the corresponding peak structural response. The proposed methodology is then applied to an actual concrete bridge wherein the different pier heights and the unrestrained transverse displacement at the abutments result in an increased contribution of the second mode. A comparison between the extended and the 'standard' DDBD is conducted, while further issues such as the proper consideration of the degree of fixity at the pier's top and the effect of the deck's torsional stiffness are also investigated. The proposed methodology and resulting designs are evaluated using nonlinear response-history analysis (NLRHA) for a number of spectrum-compatible motions. Unlike the 'standard' DDBD, the extended procedure adequately reproduced the target-displacement profile providing at the same time a good estimate of results regarding additional design quantities such as yield displacements, displacement ductilities etc., closely matching the results of the more rigorous NLRHA. However, the need for additional iterations clearly indicates that practical application of the proposed procedure is feasible only if it is fully 'automated', i.e. implemented in a software package.

KEY WORDS: displacement-based design; bridges; reinforced concrete; higher mode effects

1. INTRODUCTION

Although force-based design methods still remain the norm in existing national seismic codes, during the past decade several research groups have developed alternative, performance-based, evaluation and design procedures [1, 2], based directly on displacements and/or deformations. In this context, Moehle [3] proposed a general framework for earthquake-resistant design of structures based on drift control, with the seismic demand given by displacement response spectra, while Priestley and co-workers proposed the so-called direct displacement-based design (DDBD) for the design of fundamental mode dominated structures, which may be reduced to 'equivalent' linear single-degree-of-freedom (SDOF) systems [4 - 7]. The DDBD procedure starts from a target displacement, consistent with a deformation capacity ensured by an appropriate detailing of the structure. Estimating a reasonable value for the yield displacement, the target displacement translates into a displacement ductility demand and a corresponding equivalent damping ratio, which is used to reduce the selected displacement spectra, to account (indirectly) for nonlinear hysteretic behaviour. Entering this response spectrum with the aforementioned target displacement (expressed in terms of the displacement of the equivalent SDOF system) the effective period (secant value at target displacement) of this system is determined; subsequently, the yield strength corresponding to the previously defined peak displacement and the secant stiffness

¹ Correspondence to: A.J. Kappos, Aristotle University of Thessaloniki, Civil Engineering Department, 54124 Thessaloniki, Greece, phone: +302310995743, fax: +302310995614, email: ajkap@civil.auth.gr

1
2
3 calculated from the effective period, are found and used to apply a 'traditional' equivalent
4 lateral force design of the structure. Calvi and Kingsley [8] were the first to extend this
5 methodology to multi-degree-of-freedom (MDOF) structures which can be reduced to an
6 equivalent SDOF system using an assumed deformed configuration of the structure. For
7 buildings, this deformed configuration is that corresponding to a predefined plastic
8 mechanism and is dominated by the fundamental mode. This version of the DDBD
9 methodology, accompanied with tables for easier implementation of the procedure for
10 different performance levels, was incorporated in the SEAOC [9] recommendations (referring
11 only to buildings).
12

13 As far as bridges are concerned, the early work by Kowalsky et al. [6] dealing with isolated
14 columns modelled as SDOF systems was later extended by Kowalsky [10] and Dwairi and
15 Kowalsky [11], who introduced the effective mode shape (EMS) method to identify the
16 displacement pattern and hence the displacement profile of a bridge at the beginning of the
17 design process. Displacement pattern scenarios for continuous bridge structures subjected to
18 transverse seismic excitation were also investigated in the latter study [11] through the use of
19 nonlinear response-history analysis. Subsequently, the book by Priestley et al. [12] presented
20 a detailed treatment of the DBD procedure and its application to different structural types,
21 mainly focussing on buildings, but also addressing bridges. The primary recommendations
22 provided in this book were later codified in a draft model code [13] for the displacement-
23 based seismic design of structures. Additional issues regarding bridges, such as soil-structure
24 interaction of drilled shaft bents, skewed configurations of piers and/or abutments, conditions
25 under which DDBD can be applied using predefined displacement patterns (including the case
26 of expansion joints), and definition of stability-based target displacements that account for P-
27 Δ effects at the start of the design process were studied recently by Suarez and Kowalsky [14
28 - 17].
29

30
31 So far, the vast majority of studies performed on this topic do not consider directly higher
32 mode effects, as a result of the procedure's inherent limitation (due to the equivalent SDOF
33 approach) to structures wherein the fundamental mode dominates the response. In a recent
34 study, Adhikari et al. [18] introduced some additional considerations to account for higher
35 mode effects on flexural strength of plastic hinges in the case of long-span concrete bridges
36 with limited ductile piers. Following the suggestion of Priestley et al. [12], Adhikari et al.
37 used a response-spectrum analysis (RSA), after completion of the DDBD procedure, with two
38 different design spectra (a 5%-damped design spectrum and a design spectrum with damping
39 value obtained from the DDBD procedure) to determine the design responses (elastic and
40 inelastic respectively) at critical locations of the bridge as combinations of several modes. The
41 procedure is analogous to what has been called 'Modified Modal Superposition' by Priestley
42 [19] for cantilever wall design and 'Effective Modal Superposition' approach by Priestley and
43 co-workers [12, 20, 21] for bridge design. It is worth noting that in the latter, higher mode
44 effects were considered only for determining the design elastic responses (e.g. deck transverse
45 moment, abutment shear force), whereas inelastic responses, such as flexural strengths at
46 plastic hinge locations, were computed directly from the first inelastic mode, considering that
47 mass participation factor for the first inelastic mode was always more than 80%.
48

49
50 In view of the aforementioned limitation of DDBD and the fact that bridges are structures
51 wherein higher modes usually play a more critical role than in buildings, the present study
52 attempts to refine and extend the procedure for bridges proposed by Dwairi and Kowalsky
53 [11] and improved by the writers [22, 23], to account for higher mode effects, not only
54 regarding the proper definition of a target-displacement profile (comprising non-synchronous
55 displacements, since all significant modes are considered), but also the proper definition of
56 the corresponding peak structural response. The extended procedure proposed herein follows
57 the general approach introduced in previous studies of Chopra and Goel [24] on buildings and
58
59
60

1
2
3 Paraskveva et al. [25] on bridges, noting that these studies deal with the pushover procedure,
4 rather than with design based on elastic analysis. The efficiency of the proposed methodology
5 is then assessed by applying it to an actual bridge, whose different pier heights and the
6 unrestrained transverse displacement at the abutments result in an increased contribution of
7 higher modes. Some additional issues such as the proper consideration of the degree of fixity
8 at the pier's top and the effect of the deck's torsional stiffness are also investigated, and
9 comparisons between the extended and the 'standard' DDBD method are made. Methodology
10 and design results are finally evaluated with the aid of NLRHA.
11

12 13 14 2. A MODAL DDBD PROCEDURE FOR BRIDGES 15

16
17 An extension of the DDBD methodology to bridge structures, wherein consideration of higher
18 mode effects is deemed indispensable, is proposed herein. Procedures supplementary and/or
19 alternative to those included in the 'standard' DDBD, are presented in this section, while an
20 application of the suggested methodology to an actual bridge is given in the following section.
21 For the sake of completeness (and the benefit of the reader) all steps of the procedure
22 (including those that are essentially the same as in the Kowalsky et al. method [10, 11]) are
23 summarized in the following (see Figure 1). It has to be mentioned that the Kowalsky et al.
24 method was selected as a starting point, since the EMS method was found to be more
25 appropriate for incorporating the new developments. The EMS methodology is generally
26 deemed as the most effective procedure in the case of bridges with irregular distribution of
27 mass and stiffness that are controlled by higher mode effects; the recent study by Suarez and
28 Kowalsky [16] presents more information regarding the regularity classification of bridges
29 and its ramifications on the analysis method.
30

31
32 *Step 0 - Definition of initial input parameters:* General input parameters concerning the
33 geometry, e.g. column height and diameter (in piers with cylindrical columns), the mass
34 properties (e.g. translational mass and mass moment of inertia), and material properties are
35 defined. An initial estimate of the column cross-section is required. As a starting point, the
36 output of the dimensioning of the deck and the piers for the Ultimate and Serviceability Limit
37 States under the pertinent combinations of permanent and transient actions can be used. Then,
38 single or multiple performance levels are set as design objectives, by designating the targeted
39 damage states ('damage-based' displacements) for selected seismic hazard levels (expressed in
40 terms of elastic displacement response spectra).
41

42 *Step 1 - Selection of the displacement pattern:* The step prescribed in the 'standard' DDBD
43 procedure, involves the computation of the relative pier-to-deck stiffness (RS) and the
44 determination of whether the bridge has a rigid or a flexible displacement pattern, as
45 suggested by Dwairi et al. [11]. Given that the procedure proposed here is intended for
46 bridges where higher mode contribution should not be ignored, the flexible displacement
47 pattern scenario is adopted, disregarding the relative stiffness parameter. This means that this
48 step is essentially redundant, nevertheless it is deemed advisable to retain it, as it is always
49 useful for the designer to have a proper indication of the relative stiffness of the deck.
50

51 *Step 2 - Definition of target-displacement profiles:* The iterative EMS method is followed,
52 according to the following steps:

53 *i. Evaluation of mode shapes (Φ_j):* Due to the unavailability of the member effective
54 properties at the beginning of the process, a first estimation is required. Based on current
55 seismic design practice for bridges it can be assumed that the superstructure will respond
56
57
58
59
60

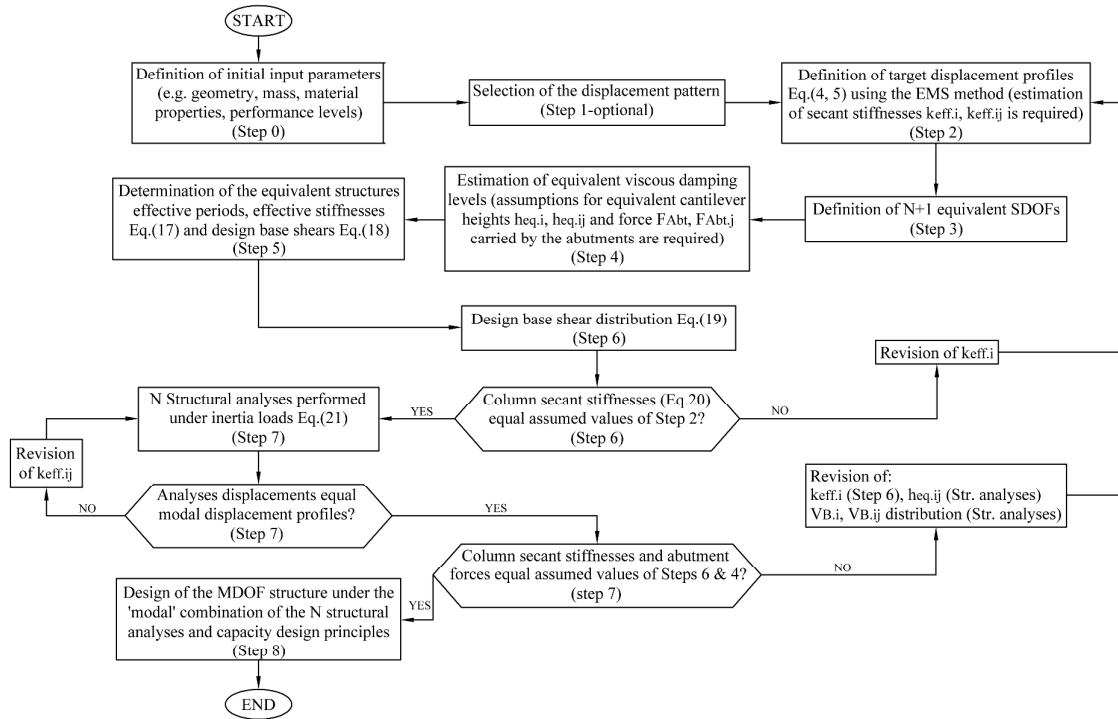


Figure 1. Modal direct displacement-based design of bridges

essentially elastically, regarding its flexural stiffness, while for its torsional stiffness it is proposed to assume 20% of the uncracked value, based on the ratios (10÷30%) of cracked-to-uncracked torsional stiffness estimated by Katsaras et al. [26]. On the other hand, it is suggested that a secant flexural stiffness based on 10% the gross section rigidity (EI_g) be used for columns expected to deform inelastically, while 60% EI_g is suggested for columns that are expected to remain below yield. The reduction in the effective axial [27] and shear [28] stiffness of the column(s) can be considered proportional to the reduction in the effective flexural stiffness. Once the structural properties have been established, the eigenvalue problem can be solved, hence the mode shapes Φ_j can be obtained.

ii. *Evaluation of modal participation factors (Γ_j):* The modal participation factors can be computed using standard procedures, i.e. Equation (1), where m represents a diagonal mass matrix and $\mathbf{1}$ is a unit vector.

$$\Gamma_j = \frac{\Phi_j^T m \mathbf{1}}{\Phi_j^T m \Phi_j} \quad (1)$$

iii. *Evaluation of peak modal displacements ($u_{i,j}$):* The peak modal displacements are computed according to Equation (2), where index i represents the DOF associated with a lumped mass, as per the inertial discretization, index j represents the mode number, $\Phi_{i,j}$ is the modal factor of joint i at mode j , and $S_{d,j}$ is the spectral displacement for mode j obtained by entering the 5%-damped design spectra with the period obtained from modal analysis.

$$u_{i,j} = \Gamma_j \Phi_{i,j} S_{d,j} \quad (2)$$

iv. *Evaluation of expected displacement pattern*: The displacement pattern (δ_i) is obtained by an appropriate combination of the peak modal displacements, such as the SRSS combination given by Equation (3); CQC combination is expected to yield better results when the natural frequencies of the participating modes in the response are closely spaced.

$$\delta_i = \sqrt{\sum_j u_{i,j}^2} \quad (3)$$

It is noted that a displacement pattern derived from the above procedure accounts for the effect of all significant modes (e.g. those needed to capture around 90% of the total mass in the transverse direction); therefore, it does not correspond to an actual inelastic deformed shape of the bridge, particularly so in the case of asymmetric systems. To obtain the target displacement profile (Δ_i), the displacement pattern given by Equation (3) is scaled in such a way that none of the member (pier or abutment) displacements exceed the target displacements obtained based on strain or drift criteria:

$$\Delta_i = \delta_i \frac{\Delta_{D,c}}{\delta_c} \quad (4)$$

where $\Delta_{D,c}$ and δ_c are the 'damage-based' displacement and the modal value at the location of the critical member, c , whose displacement governs the design, respectively. For (4) to be applied, one iteration might be needed to identify the most critical member, when this is not obvious. Finally, peak modal displacements ($u_{i,j}$) are scaled to N modal target-displacement profiles ($U_{i,j}$) utilizing the same scaling coefficient as that used to obtain the target-displacement profile in Equation (4):

$$U_{i,j} = u_{i,j} \frac{\Delta_{D,c}}{\delta_c} \quad (5)$$

An immediate consequence of the aforementioned procedure is that the combination of the N modal target-displacement profiles ($U_{i,j}$) yields the target-displacement profile (Δ_i); hence, in the case the SRSS combination rule is used:

$$\Delta_i = \sqrt{\sum_j U_{i,j}^2} \quad (6)$$

Step 3 – Definition of $N+1$ equivalent SDOF structures: These structures are established based on equality of the work done by the MDOF bridge and the equivalent SDOF structure, according to Calvi & Kingsley [8]. Each of the N SDOF structures is related to the corresponding modal target-displacement profile ($U_{i,j}$), whereas the additional SDOF is related to the target-displacement profile (Δ_i). Utilizing Equations (7) and (8), an equivalent system displacement (Δ_{sys} , $U_{sys,j}$), mass (M_{sys} , $M_{sys,j}$), and location (x_{sys} , $x_{sys,j}$) of the SDOF across the MDOF bridge deck is computed for each of the $N+1$ SDOF structures; the 'location' of the SDOF (i.e. of the masses M_{sy} or $M_{sys,i}$) coincides with the point at which the resultant of the modal forces is applied, and is one of the criteria used for checking convergence of the procedure. In Equations (7) and (8), m_i is the mass associated with joint i , and n is the number of joints as per the inertial discretization.

$$U_{sys,j} = \frac{\sum_{i=1}^n m_i U_{i,j}^2}{\sum_{i=1}^n m_i U_{i,j}}, \quad M_{sys(j)} = \frac{\sum_{i=1}^n m_i U_{i,j}}{U_{sys,j}}, \quad x_{sys,j} = \frac{\sum_{i=1}^n (m_i U_{i,j} x_i)}{\sum_{i=1}^n (m_i U_{i,j})} \quad (7)$$

6

$$\Delta_{sys} = \frac{\sum_{i=1}^n m_i \Delta_i^2}{\sum_{i=1}^n m_i \Delta_i}, M_{sys} = \frac{\sum_{i=1}^n m_i \Delta_i}{\Delta_{sys}}, x_{sys} = \frac{\sum_{i=1}^n (m_i \Delta_i x_i)}{\sum_{i=1}^n (m_i \Delta_i)} \quad (8)$$

Step 4 – Estimation of equivalent viscous damping levels: Utilizing the target displacement (Δ_i) and the modal target-displacement profiles ($U_{i,j}$), the ductility level is calculated for each member (for each of the $N+1$ profiles), according to Equation (9). Yield curvatures are estimated using Equation (10), where ε_y is the reinforcement yield strain and D is the diameter of a circular section; similar equations are provided for different section shapes [12, 28].

$$\mu_{\Delta_i} = \Delta_i / \Delta_{yi}, \text{ (or } \mu_{\Delta_i} = U_{i,j} / \Delta_{yi,j} \text{)} \quad (9)$$

$$\varphi_y = 2.25 \varepsilon_y / D \quad (10)$$

Figure 2 shows the modelling of a pier with a rigid base, whose top is monolithically connected to the deck, whereas possible moment diagrams under transverse loading are also illustrated. A pier moment diagram consists of two different components; the bending moment derived from the inertial horizontal forces F , acting on the mass centroid (G), and the bending moment induced from the eccentricity of the latter forces with respect to the shear centre, in the usual case wherein the shear centre does not coincide with the mass centroid. The final moment diagram depends on the cracked torsional stiffness of the bridge deck, the superstructure-abutment connection and the pier-superstructure relative stiffness. Likewise it is required to properly account for the degree of fixity at pier's top and hence for the pier's transverse response regarding its flexural stiffness (k_{pier}) and yield displacement ($\Delta_{y,pier}$), according to Equations (11) and (12), (referring to case (b) in Figure 1; similar relationships can be derived for the other cases).

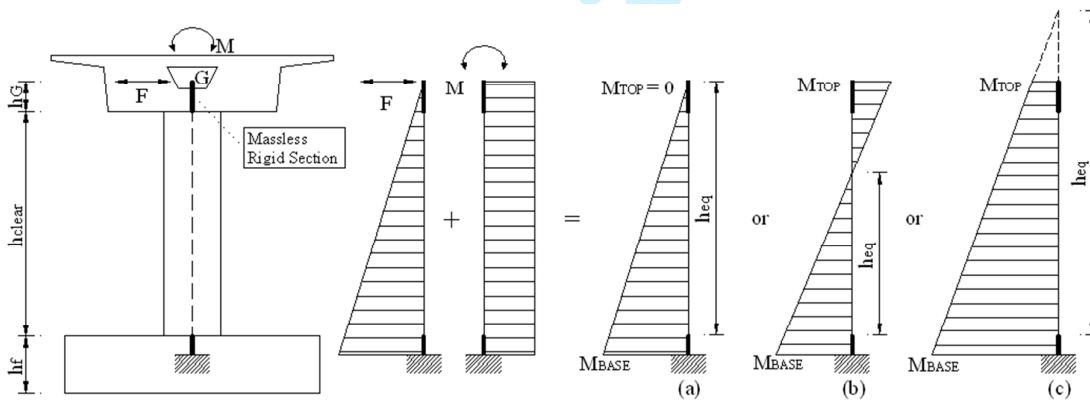


Figure 2. Pier modelling and transverse response accounting for the deck's torsional stiffness.

$$x_k = \frac{h_{eq}}{h} = \frac{h_{eq}}{h_{clear} + h_G}, k_{eq} = \frac{3EI}{h_{eq}^3}, k_{pier} = x_k k_{eq} \quad (11)$$

$$x_{\Delta_y} = \frac{L_{eq}}{L_{eff}} = \frac{h_{eq} + 0.022f_y d_{bl}}{h_{clear} + h_G + 0.022f_y d_{bl}}, \Delta_{y,eq} = \frac{\varphi_y L_{eq}^2}{3}, \Delta_{y,pier} = \frac{I}{x_{\Delta_y}} \Delta_{y,eq} \quad (12)$$

In Equations (11) and (12), $\Delta_{y,eq}$ and k_{eq} are the yield displacement and the flexural stiffness of the equivalent cantilever, E is the elastic modulus of concrete, I is the moment of inertia of

the pier cross-section (modified for cracking effects wherever necessary), d_{bl} is the longitudinal reinforcement bar diameter and $0.022f_y d_{bl}$ is the strain penetration length (where f_y is the longitudinal reinforcement yield stress in MPA). The height of the equivalent cantilever (h_{eq}) cannot be determined at the initial stage of design, therefore either preliminary structural analyses should be performed for each of the $N+1$ equivalent structures under lateral loads compatible with the corresponding profile, or an assumption that the height of the equivalent cantilever equals the height of the pier, should be made during the first iteration. The first approach is strongly recommended for the case of significant higher mode effects, since it reduces the number of iterations required to achieve convergence.

Several relationships [29 - 32] between hysteretic damping and ductility have been proposed. The one obtained by Dwairi [29] based on Takeda's hysteretic model [33], given by Equation (13), is used here. Additional elastic viscous damping (ζ_v) up to 5% should be added to the hysteretic damping in line with the approach proposed by Grant et al. [34].

$$\zeta_i = \zeta_v + \frac{50}{\pi} \left(\frac{\mu_\Delta - 1}{\mu_\Delta} \right) \% \quad (13)$$

These damping values need to be combined in some form to obtain system damping for each of the $N+1$ equivalent SDOF structures. A weighted average can be computed, as given by Equation (14), where $W_i / \sum W_k$ is a weighting factor, based on the work (W_i) done by each member (Equation (15)), according to the Kowalsky [10] approach.

$$\zeta_{sys} = \sum_{i=1}^n \left(\frac{W_i}{\sum_{k=1}^n W_k} \zeta_i \right), \quad \zeta_{sys(j)} = \sum_{i=1}^n \left(\frac{W_{i,j}}{\sum_{k=1}^n W_{k,j}} \zeta_{i,j} \right) \quad (14)$$

$$W_i = V_i \Delta_i, \quad W_{i,j} = V_{i,j} U_{i,j} \quad (15)$$

Calculation of the weighting factors obviously presupposes knowledge of member forces (V_i), which are not known at the current step. As a starting point, it can be assumed that the seismic force carried by the abutments is equal to 30% of the total seismic force carried by the bridge and column shears are inversely proportional to column heights, as illustrated by Equation (16) [10], where μ is less than one for elastic columns and equal to one for columns that have yielded. In subsequent iterations, system damping is computed using member forces obtained from structural analyses.

$$W_i = \mu_{\Delta_i} \Delta_i / h_{eq,i}, \quad W_{i,j} = \mu_{\Delta_i} U_{i,j} / h_{eq,ij} \quad (16)$$

Step 5 – Determination of the effective periods of the equivalent structures: Utilizing the $N+1$ system target-displacements ($\Delta_{sys}, U_{sys,j}$), levels of system damping ($\zeta_{sys}, \zeta_{sys,j}$), and elastic response spectra for the chosen seismic demand, the effective periods ($T_{eff}, T_{eff,j}$) of the equivalent structures are determined from the design spectrum (see Figure 4). Once the effective periods have been determined, effective stiffnesses ($k_{eff}, k_{eff,j}$) and design base shears ($V_B, V_{B,j}$) are computed by Equations (17) and (18), respectively.

$$k_{eff} = 4\pi^2 M_{sys} / T_{eff}^2, \quad k_{eff,j} = 4\pi^2 M_{sys,j} / T_{eff,j}^2 \quad (17)$$

$$V_B = k_{eff} \Delta_{sys}, \quad V_{B,j} = k_{eff,j} U_{sys,j} \quad (18)$$

Step 6 – Verification of design assumptions: Design base shears ($V_B, V_{B,j}$) are distributed in proportion to the inverse of the column height according to Equation (19), which is based on the simplifying assumption that all columns have the same diameter and longitudinal reinforcement ratio, zero post-elastic slope of the force-displacement response, mass small

enough, so that inertia forces due to self-weight can be neglected, and the same end-fixity conditions. In Equation (19) μ_i and μ_k are less than one for elastic columns and equal to one for columns that have yielded, and F_{Abt} represents the total force carried by the abutments. Member cracked section stiffnesses are computed for each of the $N+1$ profiles, using Equations (20) and are compared with values assumed at Step 2. If the values related to the target-displacement profile (Δ_i) differ significantly, computed secant stiffnesses ($k_{eff,i}$) are utilized in the EMS to obtain revised target-displacement profiles (Δ_i , $U_{i,j}$). Steps 2 to 6 are repeated by changing column secant stiffnesses until the target profile (Δ_i) stabilizes. Although a strict approach requires iteration within Steps 2 to 6 until all profiles (Δ_i and $U_{i,j}$) stabilize, the implementation of the proposed methodology in the next section indicates that whenever Δ_i stabilizes, $U_{i,j}$ also practically stabilize, hence Δ_i can be used as the sole convergence criterion.

$$V_{B,k} = (V_B - F_{Abt}) \frac{\mu_{\Delta,k}}{h_k} \left/ \sum_{i=1}^n \frac{\mu_{\Delta,i}}{h_i} \right., \quad V_{B,kj} = (V_{B,j} - F_{Abt,j}) \frac{\mu_{\Delta,kj}}{h_k} \left/ \sum_{i=1}^n \frac{\mu_{\Delta,ij}}{h_i} \right. \quad (19)$$

$$k_{eff,i} = V_{B,i} / \Delta_i, \quad k_{eff,ij} = V_{B,ij} / U_{i,j} \quad (20)$$

Step 7 - Structural analysis: Once the target-displacement profile (Δ_i) stabilizes, base shears ($V_{B,j}$) are distributed as inertia forces to the masses of the MDOF structure in accordance with the modal target-displacement profiles ($U_{i,j}$), given by Equation (21) [8]. In this equation $F_{i,j}$ are the bent inertia forces, $V_{B,j}$ are the design base shears, indices i and k refer to joint numbers, and n is the number of joints.

$$F_{k,j} = V_{B,j} \left(m_k U_{i,j} \right) \left/ \sum_{i=1}^n (m_i U_{i,j}) \right. \quad (21)$$

N structural analyses (as many as the significant modes) are performed on the bridge under the inertia loads, to obtain the 'modal' base shear for each column. Secant stiffnesses $k_{eff,ij}$ obtained from the iteration within Step 6, at which stabilization of Δ_i (hence stabilization of $U_{i,j}$ as mentioned in Step 6) was observed, should be used in each of the N structural analyses, in order to be consistent with the DDBD philosophy. Afterwards, displacements derived from the N structural analyses are compared with the corresponding profiles $U_{i,j}$. In the case of significantly different displacements, reasonable values for column secant stiffnesses are assumed and analyses are conducted until convergence is achieved. Once the displacement profiles obtained from structural analyses converge to the assumed modal target-displacement profiles, column secant stiffnesses and abutment forces from each analysis are compared with the values assumed at Step 6, at which stabilization of $U_{i,j}$ was achieved. It is reminded that during the first loop of iterations the seismic force carried by the abutments is assumed equal to 30% of the total seismic force carried by the bridge for all the $N+1$ cases. In case of significant discrepancy, the target-displacement profile is revised utilizing the EMS method and forces from structural analyses. Steps 2 to 7 are repeated, until column secant stiffnesses and abutment forces converge.

In order to perform the new loop of iterations and the new EMS in particular, previous loop secant stiffnesses ($k_{eff,i}$) (Step 6) can be assumed as the starting point. Furthermore, revised equivalent cantilever heights are computed according to the results of the N structural analyses, which were previously performed, as far as the modal target-displacement profiles ($U_{i,j}$) are concerned, whereas in the case of the target-displacement profile (Δ_i), proper values of the equivalent cantilever heights can be approximately determined by combining the peak 'modal' responses (N structural analyses). Following the same approach, the force carried by the abutments and the base shear distribution for each of the $N+1$ cases required in the

subsequent steps are determined from analysis results, instead of utilizing Equation (19), which, given the diversity of the column end-fixity conditions, is not accurate.

Step 8 - Design of the MDOF structure: The MDOF bridge is designed in accordance with capacity design principles (e.g. [28], [35]) such that the desired failure mechanism is achieved. The response quantities of design interest (displacements, plastic hinge rotations, internal pier forces) are determined by combining the peak 'modal' responses (the N structural analyses), using an appropriate modal combination rule (e.g. SRSS or CQC), and superimposing the pertinent combinations of permanent and transient actions.

3. EVALUATION OF THE PROPOSED PROCEDURE IN THE CASE OF AN EXISTING BRIDGE

3.1 Description of studied bridge

To investigate the accuracy, efficiency, and also the practicality, of the proposed procedure it was deemed appropriate to apply it to an actual bridge structure, whose different pier heights and the unrestrained transverse displacement at the abutments result in an increased contribution of the second mode. The selected structure (known as the T7 Overpass), is quite common in modern motorway construction in Europe. The 3-span structure of total length equal to 99 m (see Figure 3), is located in northern Greece and is characterized by a significant longitudinal slope (approximately 7%). The deck consists of a 10 m wide prestressed concrete box girder section with a variable geometry across the longitudinal axis of the bridge (see Figure 3). The two piers have a cylindrical cross section, a common choice for bridges both in Europe and in other areas, while the pier heights are unequal (clear column height of 5.94 and 7.93 m), due to the deck's longitudinal inclination. The deck is monolithically connected to the two piers, while it rests on its abutments through elastomeric bearings; movement in both the longitudinal and the transverse direction is initially allowed at the abutments, but transverse displacements are restrained in the actual bridge whenever the 15 cm gap shown at the bottom of Figure 3 is closed. In applying the proposed design procedure to this bridge, the gap size, as well as the characteristics of the bearings are treated as design parameters. The bridge rests on firm soil and the piers and abutments are supported on surface foundations (footings) of similar configuration.

T7 Overpass was designed using DDBD, both in the form proposed by Dwairi and Kowalsky [11], and its modified version proposed herein, for two different seismic zones. The Greek Seismic Code (EAK2000) elastic spectrum [36] for Zone II (PGA of 0.24g) and III (PGA of 0.36g) was the basis for seismic design; it corresponded to soil conditions category 'B' of the Code, which can be deemed equivalent to subsoil class 'B' of older drafts of Eurocode 8-2 and closer to 'C' in the final version of the Eurocode [35]. The bridge was designed as a ductile structure, implying that plastic hinges are expected to form in the piers, while $P-\Delta$ effects were taken into consideration. A further parameter that was investigated in applying the DDBD was the effect of the girder's torsional stiffness.

10

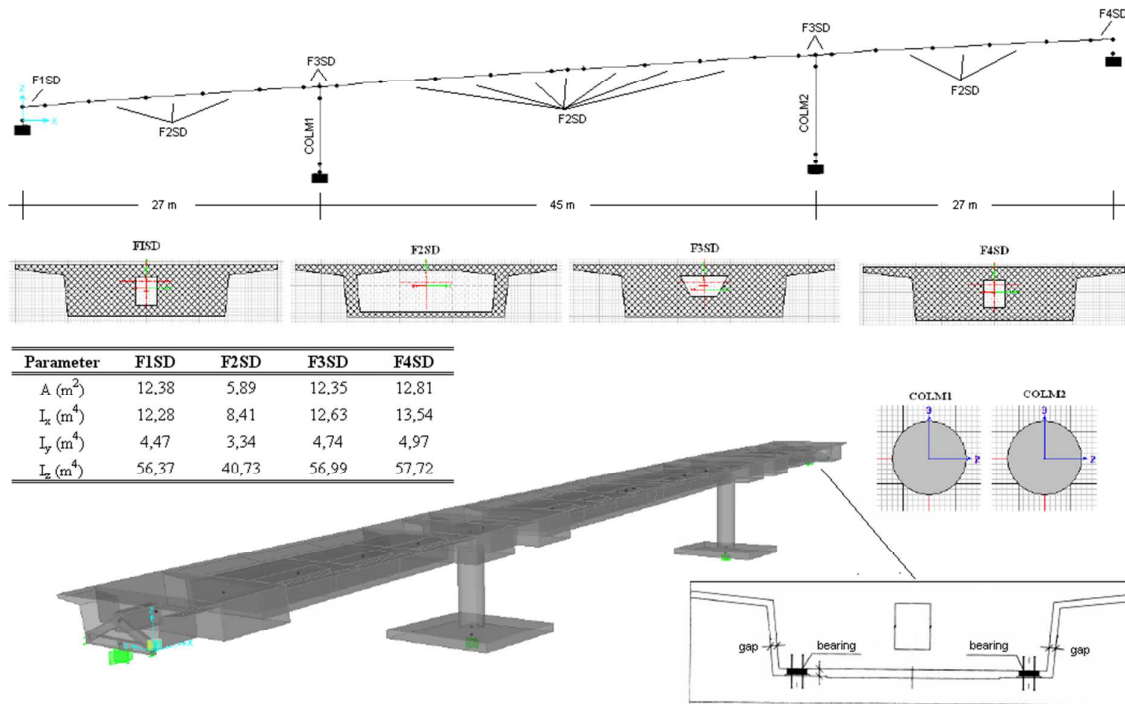


Figure 3. Layout of the bridge configuration and finite element modelling.

In the analyses presented in the following, the focus is on the transverse response of the bridge, as it is well known (e.g. [37]) that this is the response most affected by higher modes; additional analyses in the longitudinal direction were also conducted [38], however due to space limitations and the fact that longitudinal design was found to be less critical, these analyses are not presented herein. The analysis was carried out using the Ruaumoko3D software [39], whereas SAP2000 [40] was also used for additional verification; the reference finite element model (Figure 3) involved 32 non-prismatic 3D beam elements. **The elastomeric bearings present at the abutments were modelled using equivalent linear springs ('Link elements' in SAP2000, 'Spring type members' in Ruaumoko) with 6 DOF's.**

Preliminary analyses accounting for soil-structure interaction (SSI) effects, using an appropriate foundation compliance matrix, have shown that due to the relatively stiff soil formations underneath the studied bridge, SSI had little effect on the response; hence these effects were subsequently ignored in the design (and assessment) of the bridge.

3.2 'Standard' Direct Displacement-Based Design (DDBD)

A 'standard' DDBD [10, 11] was first performed, mainly to show **the limitations of the procedure, which arise** from its inherent restriction to structures wherein the fundamental mode dominates the response, as previously pointed out by Calvi & Kingsley [8]. As shown later, the transverse response of T7 Overpass, is determined by two dominant modes. A 'damage control' limit state that corresponds to a drift ratio of 3% was considered; qualitatively, 'damage control' implies that only repairable damage occurs in the columns.

The design displacement spectrum (Figure 4) was derived from the pertinent elastic acceleration response spectrum ($S_d = S_a / \omega^2$). A significant modification was made to the spectrum used for design, i.e. the corner period in S_d was taken equal to 4.0 sec, according to SEAOC's [9] recommendations, which is substantially longer than the period values of 2.0 and 2.5 specified by EC8 and the National Annex of Greece, respectively. This modification is not only in line with recent research findings, but also necessary for DDBD to be

meaningful, in the sense that short corner periods lead to small displacement values in the period range that is common to DDBD, which involves secant stiffness values at maximum displacement.

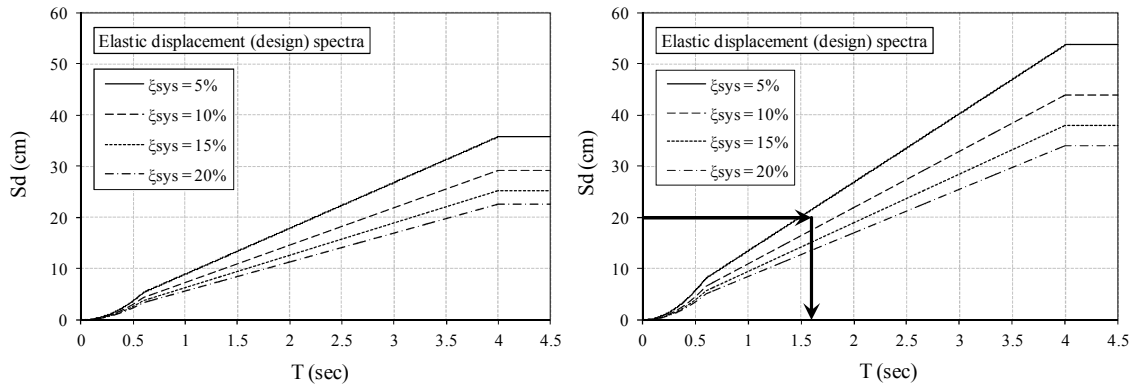


Figure 4. Elastic displacement response spectra for various damping ratios; left: Zone II (PGA=0.24g), right: Zone III (PGA=0.36g).

Moreover, the modification to the elastic acceleration spectrum, required to account for ductile response through an increased effective damping ratio, was made using the damping modifier (η) adopted in the final version of EC8 [35], i.e. Equation (22) below, where ξ_{sys} is the viscous damping ratio of the structure, expressed as a percentage.

$$\eta = \sqrt{10/(5 + \xi_{sys})} \quad (22)$$

As previously mentioned, the mechanical characteristics of the elastomeric bearings are a design parameter; hence an initial estimate is required. A rational choice of the elastomer (rubber) cross-sectional area can be made from the design for gravity loading, while, regarding the transverse modes of the bridge (Figure 5), the total thickness (t_r) of the elastomer should provide the target-displacement profile with adequate displacements at the abutments, so that the 'damage-based' displacements (Δ_D) of each column, related to the acceptable drift ratio, could be attained, and a reasonable longitudinal reinforcement ratio could be obtained for the columns. The elastomeric bearings selected herein are rectangular in shape (350 mm \times 450 mm) with t_r of 88 mm, horizontal stiffness of 2506 kN/m and equivalent viscous damping ratio equal to 5%; two bearings are placed at each abutment, as shown in Figure 3 (bottom-right). The maximum acceptable shear strain ratio (γ_u), from which the 'damage-based' displacements of the bearings are derived, is taken equal to 2.0. Introducing the 3% drift ratios for the columns and accounting for strain penetration effects, the 'damage-based' displacements of all members (piers or abutments) were defined as $\Delta_{D,Abt}=0.176$, $\Delta_{D,Col1}=0.218$, $\Delta_{D,Col2}=0.278$ m; a diameter of 2.0 m was initially assumed for the two columns (as in the original design of the bridge).

To obtain the target-displacement profile for the inelastic system, the EMS method is utilised. It is assumed that the superstructure will respond essentially elastically, as far as its flexural stiffness is concerned, while its torsional stiffness is set equal to 20% of the uncracked section torsional stiffness [26]. A secant flexural stiffness equal to 10% the gross value is applied to the columns (both of them are expected to respond inelastically), while the reduction in the effective axial and shear stiffness is considered to be proportional to the reduction in flexural stiffness. Figure 5 illustrates the target-displacement profiles derived from applying the EMS method iteratively; displacement patterns, peak modal displacements and modal mass participation factors for each mode are also shown. Convergence was

checked with regard to stabilization of the target-displacement profile or the column secant stiffness from one iteration to the next. Discrete dots on the graphs represent the points of the deck's axis passing from its mass centroid, corresponding to the centres of elastomeric bearings and columns.

The next step of the 'standard' DDBD method involves structural analysis of the bridge under the inertia loads given by Equation (21), (where, in the 'standard' procedure, U_{ij} corresponds to Δ_i), to obtain the design shear at the base of each column. In Figure 5 (bottom-right) the displacement profile derived from structural analysis Δ_i (SA1), is compared with the target-displacement profile Δ_i (EMS3). The discrepancy between the two profiles reveals one of the main deficiencies of the 'standard' DDBD, i.e. its inability to predict the peak structural response (in terms of displacements and hence internal member forces), on the basis of which design will be carried out.

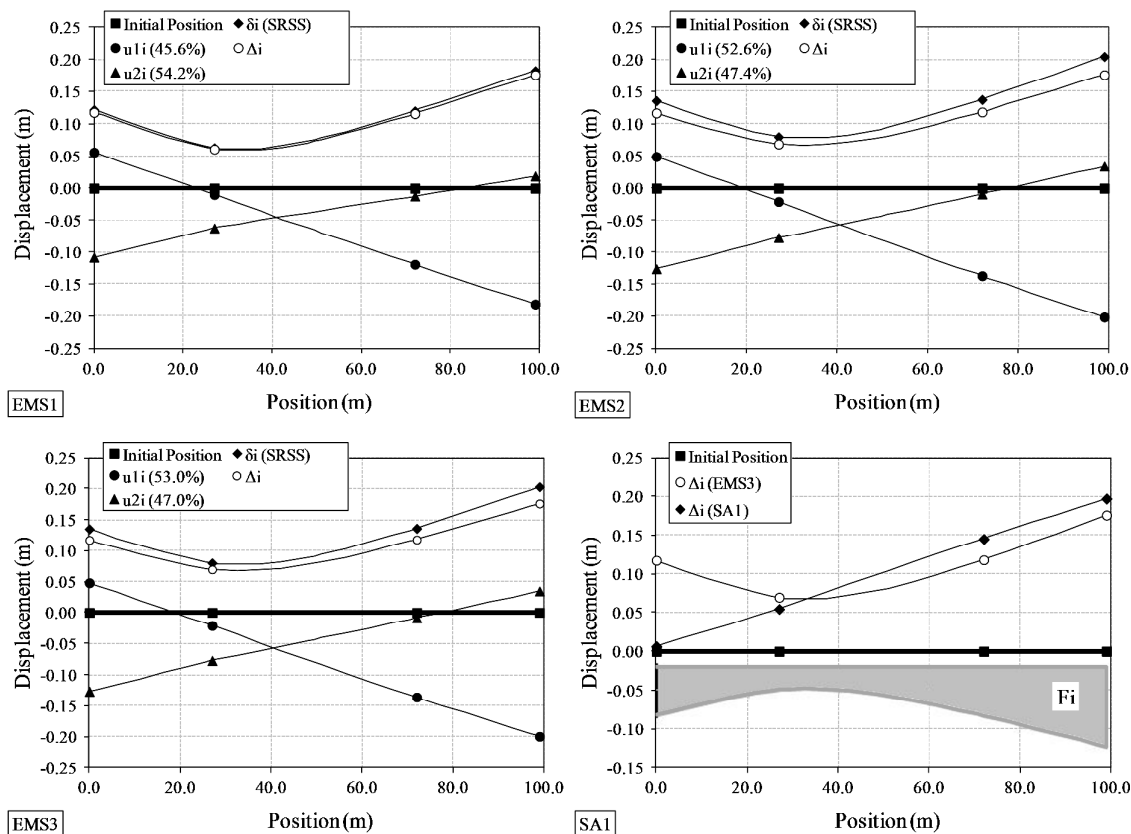


Figure 5. Displacement profiles (EMS): Peak modal displacements $u_{i,j}$, displacement pattern δ_i , and target-displacement profiles Δ_i , estimated iteratively from the EMS method. Structural analysis displacement profile (SA1) compared with target-displacement profile (base shear distribution (F_i) as inertia forces to the masses of the MDOF structure is also illustrated).

The target-displacement profile, which generally reflects the ultimate limit state (in terms of displacements) of the structural members, was constructed from the combination of the peak modal displacements (according to the SRSS rule), and then scaled in such a way that none of the member displacements exceeds the 'damage-based' design values. By following this procedure, the target-displacement profile never reflects an actual deformed shape of the structure; instead, it represents a fictitious deformed shape comprised of non-simultaneous displacements, which is deemed to reflect the peak (and non-simultaneous) structural member response. Therefore, in cases (like here) where more than one modes dominate the response, a

static structural analysis under a modal combination of seismic lateral forces such as those given by Equation (21) (whose distribution is also shown in Figure 5, bottom-right), cannot, under any circumstances, produce the target-displacement profile.

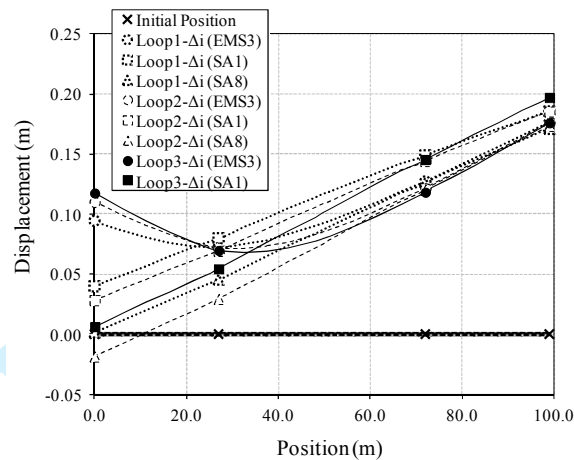


Figure 6. Target-displacement profiles $\Delta_i(\text{EMS})$, structural analysis displacement profiles (SA1) based on the secant stiffness of EMS and revised structural analysis displacement profiles (SA) that converge to the target-displacement of the critical member (i.e. Abt_2) and Col_2 , derived iteratively from the DDBD methodology.

A final remark regarding the above is that the above discrepancy in the displacement profiles is due neither to errors in the estimation of the equivalent cantilever heights nor to the approximate base shear distribution according to Equation (19). In fact, additional iterative structural analyses wherein secant stiffnesses are modified, as required by the DDBD, in this case can only lead to convergence in terms of one critical member displacement (the first member that reaches its limit state) rather than in terms of the entire target-displacement profile, which is determined from the contribution of all significant modes. To be able to compare results from the existing DDBD method with those of the proposed one, the requirement of convergence of the entire profiles was replaced by a lower requirement, namely convergence at the locations of two supporting members only, first the Abutment 2 (that has the largest displacement) and Column 2 (that is the one closest to Abt_2), and then (as an alternative) the two columns, although neither exhibits the largest design displacement. As shown in Fig. 6, several iterations (adjustments of member effective stiffness) using the converged profile from EMS ('Loop1- $\Delta_i(\text{EMS3})$ ' in the figure) fails to obtain even a rough match between the EMS displacement profile and that obtained from structural analysis ($\Delta_i(\text{SA})$ in the figure) on the left part of the bridge, while convergence is reached in the area of the left column and the left abutment (Abt_2) which are affected by the fundamental mode of the bridge (see also Figs 5 and 7). As a result of this, the design of Abutment 1 and Column 1 on the basis of the aforementioned structural analysis is not correct. Similar comments apply in the other case studied, wherein convergence was sought for the two columns.

3.3 Modal Direct Displacement-Based Design (MDDBD)

The proposed extended (modal) DDBD procedure was applied to the previous case study.

Step 0: As in the 'standard' DDBD, a 2.0 m column diameter was assumed as a starting point. However, seismic design for Zone II resulted in column longitudinal reinforcement ratios less than the minimum required by E39 [27] and other codes. Due to the fact that providing the minimum required ratio, would obscure the concepts of DDBD (regarding the

target profile, displacement ductilities etc.) and aiming at an optimum design, a 1.5 m column diameter was subsequently used. Preliminary structural analyses were performed for each of the three equivalent SDOF systems (N+1, considering the first 2 modes), under lateral loads compatible with the modal profiles and their SRSS combination, to obtain the equivalent cantilever heights and the uncracked stiffnesses ($K_{g,i}$), according to Equation (11), (see Table A1 of Appendix A). The assumed characteristics of the elastomeric bearings, the design spectrum and the 'damage-based' displacements were determined as in the 'standard' DDBD.

Steps 2 to 6: The previously described EMS methodology was applied. In order to establish the initial displacement profiles, a modal analysis was conducted where member stiffnesses were set as in the 'standard' DDBD. The peak modal displacements ($u_{i,j}$), the displacement pattern (δ_i), the target-displacement profile (Δ_i) and the modal target displacement profiles ($U_{i,j}$) were determined by Equations (2 to 5) respectively, and presented herein in Figure 7 (and Table A1), and it is clear that the abutments are the critical elements. The three equivalent SDOF systems were defined in accordance with Equations (7) and (8), and their properties are also shown in Table A1.

Once the target-displacement profiles were established, the individual member ductility values (Equations (9)) were calculated along with the corresponding equivalent viscous damping values (Equation (13)), where elastomeric bearings were assumed to respond elastically ($\xi_{Abt}=5\%$); all calculations are summarised in Table A1. Assuming that 30% of the total shear is carried by the abutments (in all 3 cases), the equivalent system damping values were obtained from Equations (14) and (16) for the first iteration and Equation (15) thereafter. The effective periods at maximum response were then obtained from Figure 4. This was then followed by the calculation of secant stiffnesses at maximum response (Equation (17)). Design base shears were calculated from Equation (18) and member shear forces from Equation (19). It is noted, that in the case of modal target-displacements with different signs, Equation (23) was used in lieu of (19) (see Table A1, Mode 2).

$$V_{B,j} - F_{Abt,j} = V_{B,lj} + V_{B,lj}, \quad V_{B,lj} / V_{B,2j} = - \left(\frac{\mu_{\Delta,1j}}{h_{eq,1j}} / \frac{\mu_{\Delta,2j}}{h_{eq,2j}} \right) \quad (23)$$

As soon as base shears for the SDOF systems are defined, the fraction of the shear carried by the abutments can be recalculated using the following equation

$$\begin{aligned} x_{Abt} &= F_{Abt} / V_B = \sum F_{Abt,i} / V_B = \sum (2k_h \Delta_{Abt,i}) / V_B \\ x_{Abt,j} &= F_{Abt,j} / V_{B,j} = \sum F_{Abt,ij} / V_{B,j} = \sum (2k_h \Delta_{Abt,i}) / V_{B,j} \end{aligned} \quad (24)$$

In Equation (24), k_h represents the bearing's horizontal stiffness (for one bearing). If the revised fractions differ significantly from the assumed values (30%), Steps 4 and 5 are repeated until fractions of x_{Abt} stabilize; in Table A1 the stabilized values of x_{Abt} are given. It is clear than in the case of seat-type abutments with bearings the design is simplified on the grounds that the shear carried by the abutment is known from the first iteration. The column secant stiffness values can be recalculated at this point since column forces and member displacements are now known (Equation (20)). This is then followed by a revised modal analysis with the new secant stiffness properties resulting into new target-displacement profiles (Δ_i , U_{ij}). In total, four iterations were needed until Δ_i stabilized. The third and fourth iterations are reported in Table A1, while the finally derived (from all iterations) profiles are illustrated in Figure 7. It is evident (from Iterations 3 and 4), that whenever Δ_i stabilizes, U_{ij} also stabilize.

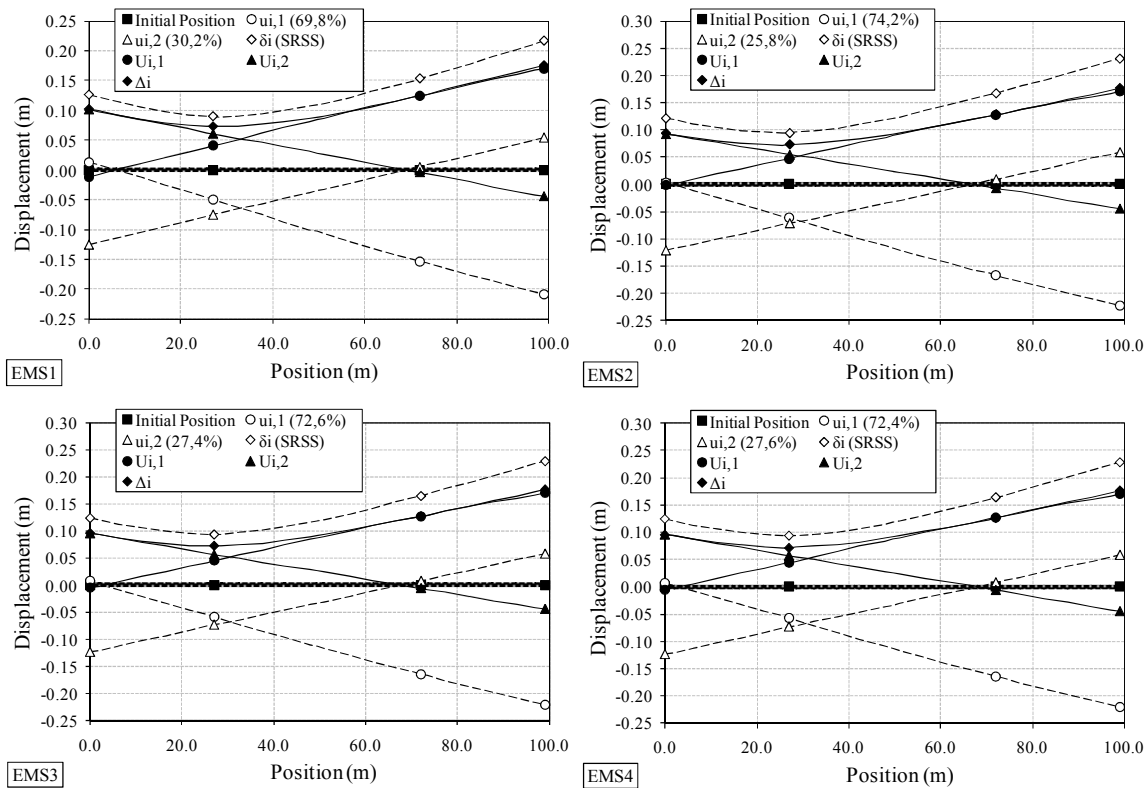


Figure 7. Displacement profiles: Peak modal displacements u_{ij} , displacement pattern δ_i , modal target-displacement profiles U_{ij} and target-displacement profiles Δ_i , derived iteratively from the EMS method.

Step 7: Once the target-displacement profile (Δ_i) stabilized, two structural analyses of the MDOF structure were performed under the inertia forces of Equation (19), utilizing the secant stiffnesses from the 4th Iteration (Mode1 and Mode2). Due to the inconsistency of the derived displacements ($U_{an,ij}$) with the corresponding modal target-displacements (U_{ij}), the two analyses were repeated with revised secant stiffnesses until convergence was achieved. Results from the structural analyses (first and last iteration) are shown in Table 1, according to which U_{i1} and U_{i2} were achieved after 8 and 5 iterations, respectively. The fact that the shear carried by the abutments in the last iteration closely matches the values obtained through EMS (Table A1, Iteration 4), results from the fact that bearing stiffness is assumed constant, determined from the initial selection of the bearing characteristics. Since the final secant stiffnesses of columns differed significantly from the assumed ones (those from Iteration 1 shown in Table 1), Steps 1 to 7 were repeated, so long as new equivalent cantilever heights and column shear distribution were defined from the structural analyses (Table 2).

The new loop of iterations attempts to reduce the discrepancy resulting from updating the equivalent cantilever height (which does not change much with respect to the initially assumed value), and the shear distribution effect according to Equation (19), but not the fraction of the shear carried by the abutments, since this is considered known, as already discussed. The results from the final iterations are summarised in the Appendix (Table A2), where the target-displacements profiles (Δ_i , U_{ij}) and the profiles derived from structural analysis ($\Delta_{an,i}$, $U_{an,ij}$) are shown. It is noted that the $\Delta_{an,i}$ is derived from the SRSS combination of $U_{an,ij}$; its divergence from Δ_i is also given.

Table 1. Summary of structural analyses.

Member	Mode 1				Mode 2				
	Abt ₁	Col ₁	Col ₂	Abt ₂	Member	Abt ₁	Col ₁	Col ₂	Abt ₂
U _{i,1} (m)	-0.006	0.044	0.126	0.170	U _{i,2} (m)	0.096	0.057	-0.006	-0.045
		<i>1st Iteration</i>					<i>1st Iteration</i>		
K _{eff,i1} /K _{g,i1} (%)		13.73	7.50		K _{eff,i2} /K _{g,i2} (%)		10.71	18.12	
U _{an,i1} (m)	-0.020	0.043	0.148	0.205	U _{an,i2} (m)	0.111	0.065	-0.005	-0.049
		<i>8th Iteration</i>					<i>5th Iteration</i>		
K _{eff,i1} /K _{g,i1} (%)		10.33	11.91		K _{eff,i2} /K _{g,i2} (%)		14.64	22.94	
U _{an,i1} (m)	-0.006	0.044	0.126	0.171	U _{an,i2} (m)	0.097	0.056	-0.006	-0.045
V _{an,i1} (m)	-34.0	910.4	1777.3	852.0	V _{an,i2} (m)	485.4	1966.0	-363.9	-224.9
x _{an,1} (%)		23.3			x _{an,2} (%)		14.0		

Table 2. Equivalent cantilever height and column shear distribution definition.

Member	Position	Str.An.8 (U _{i1})	Str.An.5 (U _{i2})	SRSS	h _{eq,i1} (m)	h _{eq,i2} (m)	h _{eq,i} (m)
Col ₁	M _{BASE} (kNm)	3412.8	6878.4	7678.5	3.75	3.50	3.54
	M _{TOP} (kNm)	-2963.4	-6890.3	7500.6			
Col ₂	M _{BASE} (kNm)	7972.2	-1264.1	8071.8	4.49	4.34	4.45
	M _{TOP} (kNm)	-8011.4	1525.3	8155.4			
Member	Position	Str.An.8 (U _{i1})	Str.An.5 (U _{i2})	SRSS	V _{i1} /(V ₁₁ +V ₂₁) (%)	V _{i2} /(V ₁₂ +V ₂₂) (%)	V _{i1} /(V ₁₁ +V ₂₁) (%)
Col ₁	V (kN)	910.4	1966.0	2166.6	33.9	122.7	54.4
Col ₂	V (kN)	1777.3	-363.9	1814.1	66.1	-22.7	45.6

Step 8: The response quantities of design interest (rotations, internal pier forces) are determined by combining the peak 'modal' responses (from the two structural analyses), using the SRSS combination rule, superimposed with the pertinent combinations of permanent and transient actions. P-Δ effects were also taken into account, and it was verified that the stability index satisfied $\theta_A \leq 0.20$. Finally, the design procedure yielded a longitudinal steel ratio of 9.8‰ and 12.4‰ for Col₁ and Col₂, respectively. The ratio of Col₁ is just slightly less than the minimum required ratio (1‰), according to E39 and the Eurocode.

The whole procedure was repeated for the case of Zone III (PGA of 0.36g), in which case a 2.0 m column diameter was selected. The results of the design procedure (final iterations only) are illustrated in Table A3 of the Appendix A. In this case the design procedure yielded a longitudinal steel ratio of 11.5‰ and 19.0‰ for Col₁ and Col₂, respectively.

Furthermore, the effect of the box girder's torsional stiffness throughout the suggested methodology was investigated. The design procedure was repeated assuming zero deck torsional stiffness, which results to cantilever action of the columns (see Figure 2(a)), and using a simplified stick model of the deck, supported on elastic translational spring elements, representing the abutments and the piers. It is clear, that such an approach simplifies the design procedure, since iterations with respect to the equivalent cantilever heights are no longer required. In Figure 8, the derived target-displacement profile (Δ_i) is compared with the corresponding profile of the previous (general) case, where deck torsional stiffness was set equal to 20% of the uncracked value. Despite the slight discrepancy in column displacements (ascribed to the different participation factors of the first two modes), the simplified design procedure yielded a longitudinal steel ratio of 42.2‰ and 62.3‰ for Col₁ and Col₂, respectively, attributed mainly to the increased required ratios of the secant-to-uncracked column stiffnesses ($K_{eff,i}/K_{g,i}$), (resulting from the significant reduction of $K_{g,i}$). It is seen that despite the fact that a zero torsional stiffness assumption simplifies the design procedure, it

also overestimates the required longitudinal steel ratios and leads to uneconomical design. Besides, in the case of concrete box girders and short to moderate span bridges, zero torsional stiffness assumption implies yielding of the deck's transverse reinforcement under the design earthquake loads [26], which is inconsistent with the current bridge design philosophy. Consequently, the above approach can only be meaningful in the case of deck typologies with low torsional stiffness and/or bearing supported superstructures.

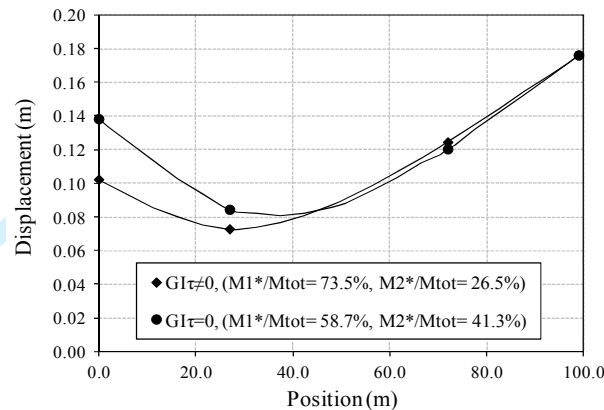


Figure 8. Target-displacement profile (Δ_i) in the case of finite and zero deck torsional stiffness (GI_T), (Zone II, $D = 1.5$ m, in both cases).

3.4 Assessment of DDBD and MDDBD using NLRHA

The existing DDBD and the proposed MDDBD procedure were assessed using nonlinear response-history analysis (NLRHA) for artificial records closely matching the design spectrum. Two different evaluation approaches were explored as described in the following.

NLRHA was first applied adopting the same assumptions as in the MDDBD. Therefore, yield curvatures obtained from Equation (10) and yield moments equal to the design requirements from Step 8 (i.e. SRSS combination of structural analysis results), were used in conjunction with a zero post-elastic slope of the moment-curvature response of the piers. This approach, hereafter referred to as the NLRHA(EI_{des}) case, was deemed necessary for evaluating the efficiency of the proposed MDDBD disengaged from parameters such as material strengths and final detailing of reinforcement. On the contrary, the second evaluation approach referred to as the NLRHA(EI_{ass}) case was meant to assess the (M)DDBD design in terms of the expected actual performance of the bridge under the design seismic actions. In particular, the design was deemed as safe if the displacement ductility demand obtained from NLRHA did not exceed the pier displacement ductility assumed in the design. This deterministic assessment requires an accurate and realistic modelling of the inelastic response to obtain the most probable response quantities. To this purpose, moment-curvature analyses based on mean values for material properties and the final detailing of reinforcement, were performed for each pier section utilizing the in-house developed computer program RCCOLA.NET. The assessment in both cases focussed mainly on the target-displacement profiles and on design quantities such as yield displacements, displacement ductilities, stiffnesses, and magnitude of forces developed in critical members of the bridge.

Nonlinear analyses were carried out using Ruaumoko3D [39]; appropriate nonlinear beam members that in general follow the concept of the one-component model, were introduced in the finite element model (Figure 3) to model the inelastic response of the piers (instead of beam-column members, since there are no changes in axial force that affect the yield

1
2
3 moments related to the transverse response of this straight bridge). Herein, the modified
4 Takeda degrading-stiffness hysteresis rules [39], (with parameters $\alpha = 0.5$ and $\beta = 0$ as
5 assumed for design [11] to estimate ξ_i), were adopted.

6
7 Since the primary objective of the assessment was the study of the transverse response of
8 the bridge under a seismic excitation which matches as closely as feasible the 'design
9 excitation' (i.e. the design spectrum), two sets of NLRHA (EI_{des} , EI_{ass}) were performed for
10 each design case (Zone II, III), using five artificial records, generated with the computer
11 program ASING [41] to fit the elastic design S_a spectra. Response history analyses were
12 performed using the unconditionally stable implicit Newmark constant average acceleration
13 method [39], while (after some pilot analyses) Rayleigh damping based on tangent stiffness
14 was selected. The integration time step was set equal to 0.01 sec, after trial analyses.

15 In Figure 9 the target-displacement profiles and the displacement profiles obtained from
16 structural analyses within the **DDBD and MDDBD procedures** are compared with the
17 displacement envelopes from the NLRHA(EI_{des}) and (EI_{ass}) cases; the deck displacements
18 shown in the figures as the NLRHA case are the average of the maximum displacements
19 recorded in the structure during the five RHA's of each set. **It is observed that agreement of
20 the DDBD design profiles with the corresponding response-history results is not satisfactory,
21 since the NLRHA profile is closer to the target-displacement profile Δ_i (derived from EMS
22 and accounting for higher mode effects) instead of the displacement profile obtained from
23 structural analysis, on the basis of which design is carried out. On the other hand, the
24 MDDBD target-displacement profiles are closer to that obtained from NLRHA(EI_{des}), more
25 so in the case of Zone II. The main difference between MDDBD and NLRHA(EI_{des}) is noted
26 towards the abutments of the bridge (critical members in design), with differences
27 diminishing in the area of the piers. These differences should be attributed to the inherent
28 inability of elastic design methodologies that are based on modal analysis (e.g. response
29 spectrum analysis) to capture the modification of the dynamic characteristics of the structure
30 during the successive formation of plastic hinges. The proposed procedure attempts to capture
31 the maximum probable response at a given performance level (after the formation of plastic
32 hinges) based on a statistical combination (e.g. SRSS) of the peak 'modal' responses.
33 Additional sets of linear response history analyses (LRHA) for the case '(EI_{des})' were
34 performed to support the above statement. In particular, column stiffnesses were set equal to
35 secant stiffnesses corresponding to maximum displacements obtained from previously run
36 nonlinear analysis (i.e. NLRHA(EI_{des})). The displacement envelopes resulting from these
37 analyses indicate the contribution of the first two modes with similar participation factors as
38 those obtained from the EMS method (Figure 9). The NLRHA(EI_{ass}) case is also given in
39 Figure 9 to underline the divergence (in terms of displacement profiles) arising when pier
40 overstrength, due to the use of mean values for material properties and consideration of strain-
41 hardening of steel reinforcement, is considered.**

42
43
44
45
46
47
48
49
50
51
52
53
54
55
56
57
58
59
60

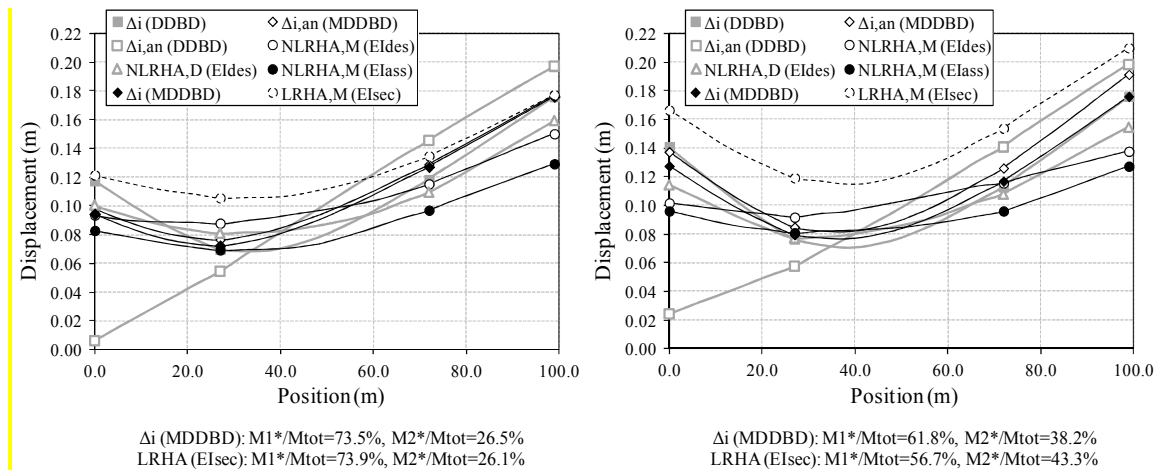


Figure 9. Nonlinear response history maximum displacements for evaluation cases NLRHA(EI_{ides}), (EI_{ass}) and linear response history maximum displacements for evaluation case NLRHA(EI_{ides}). Left: Zone II (PGA=0.24g); Right: Zone III (PGA=0.36g), compared with target-displacements profiles (Δ_i) and displacement profiles obtained from structural analyses ($\Delta_{i,an}$) according to DDBD (D) and Modal DDBD (M).

Similar conclusions are drawn with respect to the other design quantities; yield displacements, displacement ductilities, stiffnesses, ultimate member shears, bearing shear strain and column drift ratios obtained from NLRHA were compared with those estimated at the design stage. Figure 10 (supplemented by Table 3, as far as the results related to the MDDBD are concerned) illustrates the correlation in the above quantities, in the case of Zone II. Again, curves shown in the figures as the NLRHA case are the average of the quantities recorded in the structure during the five RHAs, either at the time step each member enters the inelastic range (displacement and shear values at the instant wherein the bending moment at the critical section first reaches the yield bending moment of EI_{des}/EI_{ass} case) or at the time step of maximum response. V- Δ curves shown as MDDBD were drawn based on the method's assumptions (i.e. assuming zero post-elastic slope of the shear force vs. displacement response and yield displacement according to Equation (12)) and the results of structural analyses (SRSS combination), therefore minor differences may be observed in the design quantities of Table 3 and the corresponding values of Table A2. It is clear that, contrary to the DDBD, MDDBD predicts very well, (i.e. matches closely the values from the NLRHA(EI_{des}) case), the quantities related to member ultimate response (shear forces, displacements and secant stiffnesses at maximum response), which implies the effectiveness of the equivalent cantilever approach in capturing the degree of fixity at the top of the piers, and the base shear distribution approach according to the results of structural analysis. Differences in the quantities related to pier yield are mainly attributed to the estimation of the yield curvature according to the semi-empirical Equation (10) and the computation of the equivalent cantilever height according to moment diagrams at maximum response instead of the response at the time of yielding. The resulting underestimation of the equivalent cantilever height (also addressed in Table 3) contributes to underestimation of yield displacements and overestimation of stiffnesses and shears related to pier yield. It is worth mentioning that DDBD yields similar results with MDDBD as far as Column 2 is concerned (whose design is governed by the first mode), whereas it overestimates the 'second mode-based' response of Column 1.

As previously mentioned, the results of the NLRHA(EI_{ass}) case were used to verify the reliability of the proposed design method in terms of ductility demand. Both designs were found to be safe, since required ductilities values for Zones II and III are always lower than

the design ductilities (see Table 3 for case of Zone II). Figure 10, also illustrates the effects of overstrength on the V-Δ pier response.

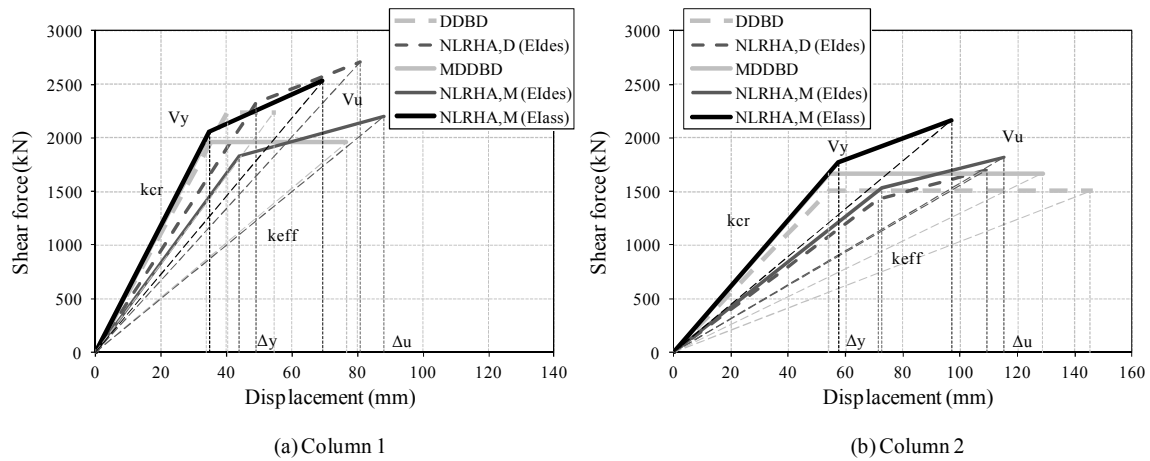


Figure 10. Member shear force vs. displacement curves derived from direct displacement-based design (DDBD), modal direct displacement-based design (MDDBD) and nonlinear response history analyses (NLRHA) in the case of Zone II (PGA=0.24g) design.

Table 3. Design quantities in the case depicted in Figure 10.

Member	Abutment 1			Abutment 2			Column 1			Column 2		
	Case	MDDBD	NLRHA (E _{I_{des}})	NLRHA (E _{I_{ass}})	MDDBD	NLRHA (E _{I_{des}})	NLRHA (E _{I_{ass}})	MDDBD	NLRHA (E _{I_{des}})	NLRHA (E _{I_{ass}})	MDDBD	NLRHA (E _{I_{des}})
Δ _y (mm)							34	44	35	54	73	58
V _y (kN)							1958.6	1828.8	2060.0	1668.5	1529.2	1769.4
Δ _u (mm)	98	94	83	177	141	129	77	88	69	129	115	97
V _u (kN)	491.3	469.0	415.2	885.4	707.7	647.6	1958.6	2196.2	2529.2	1668.5	1817.8	2166.4
K _h (kN/m)	5011.4	5011.4	5011.4	5011.4	5011.4	5011.4						
K _{cr} (kN/m)							58072.9	41559.9	59195.4	30860.9	21025.1	30736.9
K _{eff} (kN/m)							25576.3	24984.6	36493.2	12952.7	15774.0	22342.8
μ _Δ							2.27	2.00	1.99	2.38	1.58	1.68
γ ^o (γ _u =2.0)	1.11	1.06	0.94	2.01	1.60	1.47						
Col. Drift (%)							1.05	1.21	0.95	1.39	1.24	1.05
h _{eq} (m)							3.43	3.79	4.43	4.39	5.02	5.61

4. CONCLUSIONS

An existing displacement-based methodology (DDBD) was extended here to account for higher mode effects in the case of bridges. Its feasibility and accuracy were evaluated by applying it to an actual bridge wherein two modes dominate the transverse response. The key issue in this extension was the proper definition of N+1 target-displacement profiles and equal in number equivalent SDOF structures for applying the EMS method and estimating the peak 'modal' earthquake forces. The peak 'modal' response was then obtained by conducting N structural analyses (as many as the significant modes) on the MDOF. Additional issues addressed included the pier columns' degree of fixity, introducing the concept of the equivalent cantilever heights, and the base shear distribution according to the results of structural analysis. The significance of a rational consideration of the superstructure torsional stiffness throughout the design procedure was also illustrated.

1
2
3 By evaluating both DDBD and MDDBD in the light of NLRHA results for the
4 aforementioned bridge, it was concluded that:

- 5 • The DDBD method failed to reproduce the target-displacement profile (Δ_i), which was
6 anticipated given the fact that the latter represents a fictitious profile consisting from non-
7 synchronous displacements, and eventually reflects the peak (and non-synchronous)
8 structural member response. On the contrary, MDDBD is intrinsically capable of meeting
9 this goal by producing the target-displacement-profile (Δ_i) and hence the peak structural
10 response.
 - 11 • MDDBD provided displacement profiles that cannot in general account for the
12 modification of the structural dynamic characteristics during the formation of plastic
13 hinges; nevertheless, it can estimate the probable response at a given performance level
14 (after the formation of plastic hinges) based on a statistical combination (e.g. SRSS) of
15 peak 'modal' responses. Additional design quantities (displacements, shear forces and
16 secant stiffnesses) related to the ultimate response of piers closely matched the results of
17 the more rigorous NLRHA, indicating at the same time the validity of the equivalent
18 cantilever concept and base shear distribution according to the results of structural analysis.
 - 19 • Deterministic assessment of the design indicated that MDDBD resulted in safe design in
20 terms of pier displacement ductility demand.
 - 21 • Investigation of the effect of deck torsional stiffness in the suggested methodology revealed
22 the significance of a properly selected value according to modern bridge design philosophy.
23 In contrast, the simplified design procedure, based on the assumption of simple cantilever
24 column behaviour under lateral earthquake forces, resulted in significantly overestimated
25 longitudinal steel ratios and can only be acceptable in the case of deck typologies with low
26 torsional stiffness.
 - 27 • In the light of the results obtained for the studied bridge, MDDBD can be further simplified
28 with respect to the required iterations in the EMS method (Steps 2 to 6). Given that
29 whenever the target-displacement profile Δ_i stabilized, modal target displacement profiles
30 $U_{i,j}$ also stabilized, Δ_i (and hence the characteristics of the corresponding SDOF) can be
31 used as the sole convergence criterion during Steps 2 to 6. $U_{i,j}$ and hence the remaining
32 SDOFs should be used only in the last iteration, in order to define the peak 'modal'
33 earthquake forces (base shears of Equation (18)). This simplification reduces the
34 computational cost of the method.
 - 35 • More work is clearly required to further investigate the effectiveness of MDDBD by
36 applying it to bridge structures with higher mode contribution (even more significant than
37 in the bridge studied here) **and/or curved in plan bridges**, since MDDBD is expected to be
38 more valuable for the proper estimation of the actual inelastic response and hence for the
39 efficient design of bridges with significant higher modes. Further investigation is also
40 required in the case of different abutment configurations (i.e. superstructure's transverse
41 displacement restrained at the abutments through seismic links, causing activation of the
42 abutment-backfill system), wherein the shear carried by the abutment is not known during
43 the design procedure.
 - 44 • The MDDBD method proposed herein, as a rule requires a substantial number of iterations;
45 therefore an implementation of the proposed procedure in a software package would
46 significantly increase its usefulness in practical design.
- 47
48
49
50
51
52
53
54
55
56
57
58
59
60

ACKNOWLEDGEMENTS

The contributions of Asst. Prof. A. Sextos and Dr. I. Moschonas (from the Civil Engineering Department of the Aristotle University of Thessaloniki) to the computational aspects of this work are gratefully acknowledged.

REFERENCES

1. Sullivan TJ, Calvi GM, Priestley MJN, Kowalsky MJ. The limitations and performances of different displacement based design methods. *Journal of Earthquake Engineering* 2003; **7**(1):201–241.
2. fib (Fédération Internationale du Béton). *Bulletin No.25: Displacement-based seismic design of reinforced concrete buildings*, Lausanne 2003.
3. Moehle JP. Displacement based design of RC structures subjected to earthquakes. *Earthquake Spectra* 1992; **8**(3):403–428.
4. Priestley MJN. Myths and fallacies in earthquake engineering – Conflicts between design and reality. *Proceedings of the Tom Paulay Symposium – Recent Developments in Lateral Force Transfer in Buildings*, San Diego, 1993:229–252.
5. Priestley MJN. Performance based seismic design. *Proceedings of the 12th World Conference on Earthquake Engineering*, Auckland, NZ, 2000; Paper No.2831.
6. Kowalsky MJ, Priestley MJN, MacRae GA. Displacement-based design of RC bridge columns in seismic regions. *Earthquake Engineering and Structural Dynamics* 1995; **24**(12):1623–1643.
7. Kowalsky MJ, Priestley MJN. Experimental verification of direct displacement-based design and development of approach for multiple degree of freedom systems. *Proceedings of the National Seismic Conference on Bridges and Highways, Progress in Research and Practice*, Federal Highway Administration, Sacramento, CA, 1997;651–665.
8. Calvi GM, Kingsley GR. Displacement based seismic design of multi-degree-of-freedom bridge structures. *Earthquake Engineering and Structural Dynamics*. 1996; **24**:1247–1266.
9. Seismology Committee of Structural Engineers Association of California (SEAOC). *Recommended lateral force requirements and commentary (Blue Book)*, Sacramento, California, 1999.
10. Kowalsky MJ. A displacement-based design approach for the seismic design of continuous concrete bridges. *Earthquake Engineering and Structural Dynamics* 2002; **31**:719–747.
11. Dwairi H, Kowalsky M. Implementation of inelastic displacement patterns in direct displacement-based design of continuous bridge structures. *Earthquake Spectra* 2006; **22**(3):631–662.
12. Priestley MJN, Calvi GM, Kowalsky MJ. *Displacement-based seismic design of structures*. IUSS Press, Pavia, Italy, 2007.
13. Calvi GM, Sullivan TJ. *A model code for the displacement-based seismic design of structures*. IUSS Press, Pavia, Italy, 2009.
14. Suarez V, Kowalsky MJ. Displacement-based seismic design of drilled shaft bents with soil-structure interaction. *Journal of Earthquake Engineering* 2007; **11**(6):1010–1030.
15. Suarez VA. *Implementation of direct displacement-based design for highway bridges*. Ph.D. dissertation, North Carolina State University, Raleigh, NC, 2008.
16. Suarez VA, Kowalsky MJ. *Direct displacement-based design as an alternative method for seismic design of bridges*. SP-271CD: Structural Concrete in Performance-Based Seismic Design of Bridges CD-ROM, ACI 2010, Order code: SP271CD.
17. Suarez VA, Kowalsky MJ. A stability-based target displacement for direct-displacement-based design of bridge piers. *Journal of Earthquake Engineering* 2011; **15**(5):754–774.
18. Adhikari G, Petrini L, Calvi GM. Application of direct displacement based design to long span bridges. *Bulletin of Earthquake Engineering* 2010; **8**(4):897–919.
19. Priestley MJN. *Myths and fallacies in earthquake engineering, Revisited*. The Mallet Milne Lecture. IUSS Press, Pavia, Italy, 2003.
20. Alvarez Botero JC. *Displacement-based design of continuous concrete bridges under transverse seismic excitation*. M.Sc. Dissertation, European school for advanced studies in reduction of seismic risk (Rose School), University of Pavia, Italy, 2004.
21. Ortiz Restrepo JC. *Displacement-based design of continuous concrete bridges under transverse seismic excitation*. M.Sc. Dissertation, European school for advanced studies in reduction of seismic risk (ROSE School), University of Pavia, Italy, 2006.

22. Kappos AJ, Gidaris I, Gkatzogias KI. An improved displacement-based design procedure for concrete bridges. *Proceedings of the 3rd International Conference on Seismic Retrofitting*, Tabriz, Iran, 20-22 October, 2010.
23. Kappos AJ, Gkatzogias KI, Gidaris IG. An improved displacement-based seismic design methodology for bridges accounting for higher mode effects. *Proceedings of the 3rd International Conference on Computational Methods in Structural Dynamics and Earthquake Engineering*, Keynote lecture, Corfu, Greece, 26-28 May, 2011; Paper No.256.
24. Chopra AK, Goel RK. A modal pushover analysis procedure for estimating seismic demands for buildings. *Earthquake Engineering and Structural Dynamics* 2002; **31**(3):561–582.
25. Paraskeva TS, Kappos AJ, Sextos AG. Extension of modal pushover analysis to seismic assessment of bridges. *Earthquake Engineering and Structural Dynamics* 2006; **35**(11):1269-1293.
26. Katsaras CP, Panagiotakos TB, Koliass B. Effect of torsional stiffness of prestressed concrete box girders and uplift of abutment bearings on seismic performance of bridges. *Bulletin of Earthquake Engineering* 2009; **7**:363–375.
27. Ministry of Public Works of Greece. *Guidelines for earthquake resistant design of bridges (E39)*, Athens, 2007 (in Greek).
28. Priestley MJN, Seible F, Calvi GM. *Seismic design and retrofit of bridge structures*. Wiley: New York, 1996.
29. Dwairi HM. *Equivalent damping in support of direct displacement-based design with applications to multi-span bridges*. Ph.D. dissertation, North Carolina State University, Raleigh, NC, 2004.
30. Blandon CA, Priestley MJN. Equivalent viscous damping equations for direct displacement-based design. *Journal of Earthquake Engineering*. 2005; **9**:257-278.
31. Guyader C, Iwan WD. Determining equivalent linear parameters for use in a capacity spectrum method of analysis. *Journal of Structural Engineering*. 2006; **132**(1):59-67
32. Dwairi HM, Kowalsky MJ, Nau JM. Equivalent Damping in Support of Direct Displacement-Based Design. *Journal of Earthquake Engineering*. 2007; **11**:512–530.
33. Takeda T, Sozen M, Nielsen N. Reinforced concrete response to simulated earthquakes. *Journal of the Structural Division, ASCE*, 1970; **96**(12):2557–2573.
34. Grant DN, Blandon CA, Priestley MJN. *Modeling inelastic response in direct displacement-based design*. Report No. ROSE 2004/02, European School of Advanced Studies in Reduction of Seismic Risk, Pavia, Italy, 2004.
35. CEN (Comité Européen de Normalisation). *Eurocode 8: design of structures for earthquake resistance—Part 2: Bridges*, Brussels, 2005.
36. Ministry of Public Works of Greece. *Greek seismic code-EAK 2000*, Athens, 2000 (amended June, August 2003, March 2010) (in Greek).
37. Fischinger M, Beg D, Isakovic T, Tomazevic M, Zarnic R. Performance based assessment—from general methodologies to specific implementations. *International Workshop on PBSDB, Bled, Slovenia 2004*; 293–308 (published in PEER Report 2004-05 (UC Berkeley)).
38. Gkatzogias KI. *Displacement-based seismic design of an RC bridge*. M.Sc. dissertation, Aristotle University of Thessaloniki, 2009, (in Greek).
39. Carr AJ. *Ruaumoko 3D: Inelastic dynamic analysis program*. University of Canterbury, Christchurch, New Zealand, 2006.
40. Computers and Structures Inc. *SAP2000: Three dimensional static and dynamic finite element analysis and design of structures*. Computers and Structures Inc.: Berkeley, CA, 2009.
41. Sextos AG, Pitilakis KD, Kappos AJ. Inelastic dynamic analysis of RC bridges accounting for spatial variability of ground motion, site effects and soil-structure interaction phenomena. Part 1: Methodology and analytical tools. *Earthquake Engineering and Structural Dynamics* 2003; **32**(4):607–627.

APPENDIX A: DETAILS OF THE MODAL DDBD CASE STUDY

An Appendix including tables related to the case study presented in section 3.3 'Modal Direct Displacement-Based Design (MDDBD)', presenting details of selected steps of the design iterations, [can be found here](#).